CONF-9505264--7

UCRL-JC-121453
PREPRINT

Performance modeling of Beamlet

J. M. Auerbach
J. K. Lawson
M. D. Rotter
R. A. Sacks
B. W. Van Wonterghem
W. H. Williams

This paper was prepared for submittal to the
1st Annual International Conference on
Solid-State Lasers for Application to Inertial Confinement Fusion (ICF)
Monterey, CA
May 30-June 2, 1995

June 27, 1995

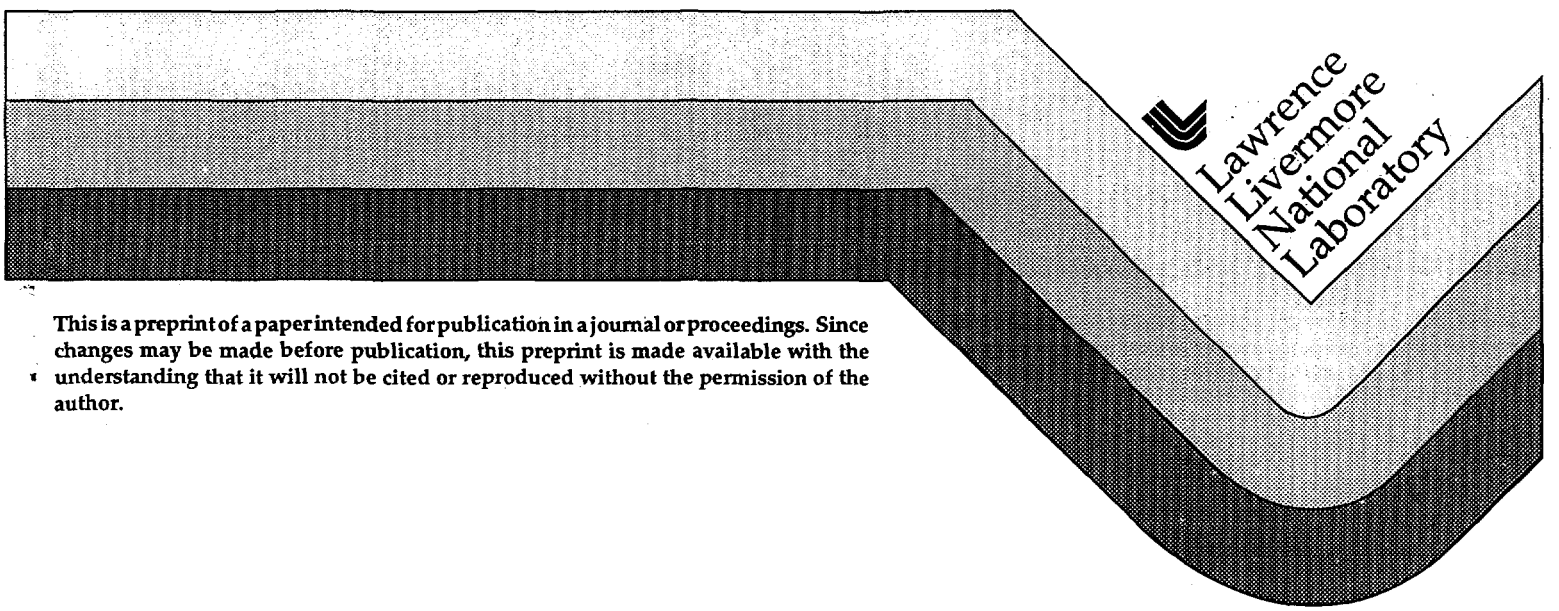

DISCLAIMER

Performance modeling of Beamlet

Jerome M. Auerbach, Janice K. Lawson, Mark D. Rotter
Richard A. Sacks, Bruno W. Van Wonterghem, Wade H. Williams

Lawrence Livermore National Laboratory
PO Box 5508
Livermore, California 94550

ABSTRACT

Detailed modeling of beam propagation in Beamlet has been made to predict system performance. New software allows extensive use of optical component characteristics. This inclusion of real optical component characteristics has resulted in close agreement between calculated and measured beam distributions.

2. MODELING CAPABILITIES

Modeling of the Beamlet laser system was utilized in each step of its activation to full output. From simulations of laser operation, one can predict possible damage situations as well as output parameters such as conversion efficiency and beam focusability. Modeling calculations are accomplished with a new family of propagation and frequency conversion codes. This paper will describe the capabilities and results from the propagation codes. The propagation codes contain standard algorithms for modeling solid-state laser systems. The physical processes corresponding to these algorithms are paraxial diffraction, nonlinear index phase retardation,[1] and saturable gain (Frantz-Nodvik) amplifiers.[2] However it is the capability of these codes to include extensive characteristics of real optical components that gives them their unique capability. These characteristics are input to the codes by files that are either in ASCII or binary format. Measured characteristics such as amplifier slab gain profiles and small scale phase aberrations of optical components are critical in determining beam shapes and modulation level. In fact it was the initial modeling of Beamlet with spatial dependent gain profiles that indicated the need for a "gain compensating transmission mask" in the front-end to produce a spatially flat spatial beam distribution at the system output.

Gain profiles used in the modeling were measured using modules of the Beamlet slab amplifier set in different configurations.[3] Three types of gain profiles are defined as shown in Figure 1: one for an interior slab (not on the end of an amplifier module); one for an end slab in the "X" configuration, and one for an end slab in the "Diamond" configuration. The "X" and "Diamond" nomenclature is based on whether the four end slabs in adjacent amplifier modules appear to have the form of an X or diamond. In addition to the gain profile measurements, the pump-induced aberrations were determined for these three slab types. Small probe beams were sent through the laser slabs when pumped and the resulting beam steering was measured. The corresponding phase aberrations are obtained from the steering angles by integration.

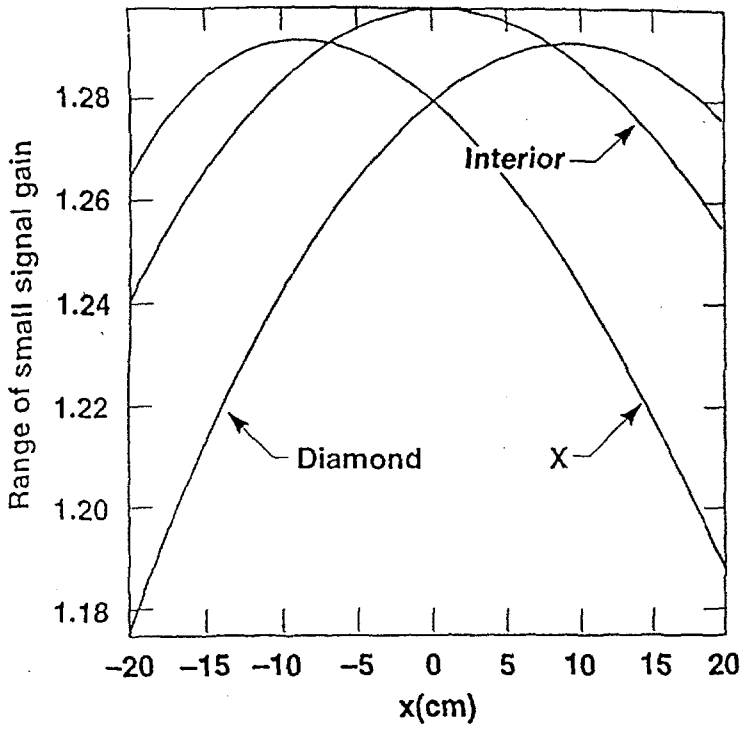

Figure 1. The gain profiles for the Interior, Diamond, and "X" amplifier slabs. Profiles are fits to measured data and are for 1 transverse dimension only.

Propagation modeling of Beamlet starts in the front end at the serrated aperture apodizer and ends at the input of the frequency converter. The "propagation path" is illustrated in the schematic diagram of Figure 2. Note that there are two 4-pass amplifiers in the system: the 4 pass rod amplifier in the front end and the 4 pass 11 slab amplifier in the main cavity. The initial beam apodization is accomplished with a serrated aperture/spatial filter apodizer[4] followed by a gain compensator mask. This mask has a 3:1 parabolic shape. The propagation codes allow an arbitrary mask shape to be supplied as input in a file.

Figure 2. A schematic diagram of the propagation path used for the modeling. The 1ω laser pulse starts at the serrated aperture apodizer and ends at the input of the frequency converter.

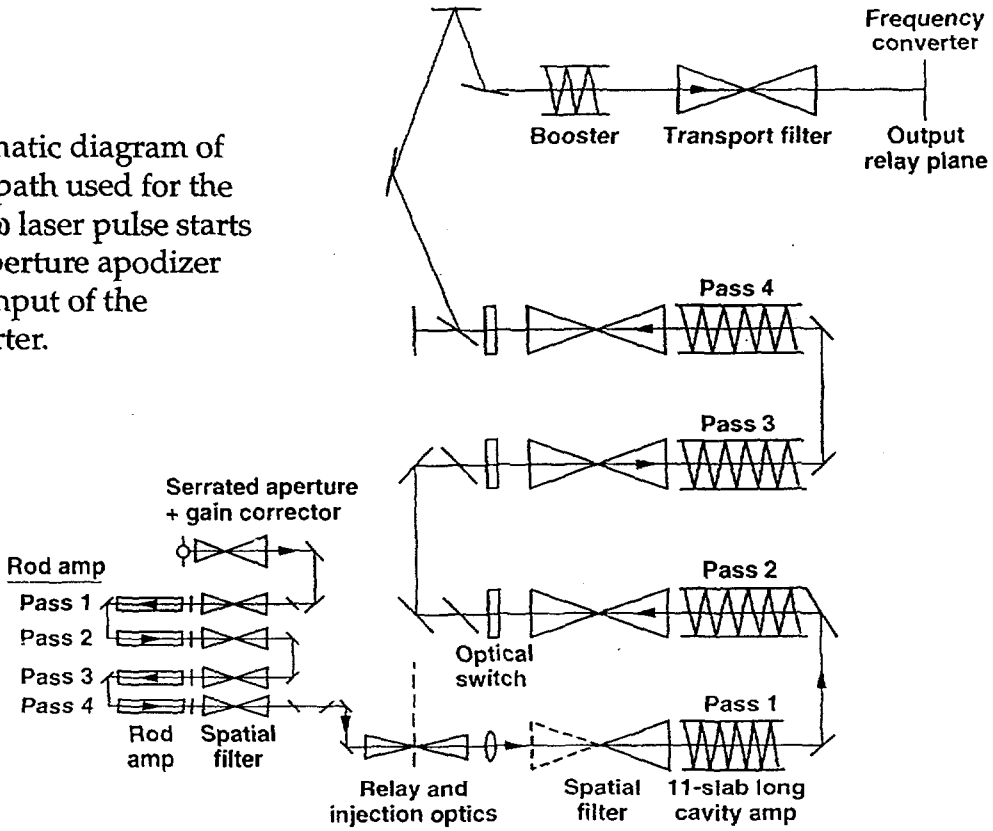

Phase maps of optical component static interferograms are either purely measured data or maps synthesized from measured data. Phase shifting interferometry is used to obtain interferograms of the optical components. These are either for the component's full aperture or in most cases for different size sub-apertures. These different sizes allow one to obtain phase maps over a wide range of phase ripple scale lengths. Creating a full aperture phase map from these sub-aperture interferograms is accomplished using either simple replication or by combining power spectral distributions (PSD) for the sub-apertures. Replication is used for periodic or coherent structure phase maps and the PSD method is used for phase maps with random structures. A full aperture phase map based on PSD's is created from sub-aperture interferogram data as follows.

(1) PSD's are calculated for the sub-aperture phase data. Sub-apertures are chosen for minimal spectral overlap.

(2) For each sub-aperture, a spectrum is made in which the spectral components are assigned a random phase and an amplitude equal to the square root of the corresponding PSD value.

(3) Each new sub-aperture spectrum is inverse Fourier Transformed on the full aperture grid. Grid resolution may result in loss of the highest spatial frequency information in the smallest sub-aperture.

(4) The full-aperture phase maps corresponding to each sub-aperture are summed to give the complete full-aperture phase map.

Figure 3 shows a contour plot of a calculated full-aperture phase map for an amplifier slab.

Phase maps are typically defined on a 512 X 512 grid of lengths 40 cm x 40 cm. The grid increment is thus 0.8 mm. The maximum spectral angle thus resolvable on this grid is 1.2 mrad at a laser wavelength of 1.053 μm.

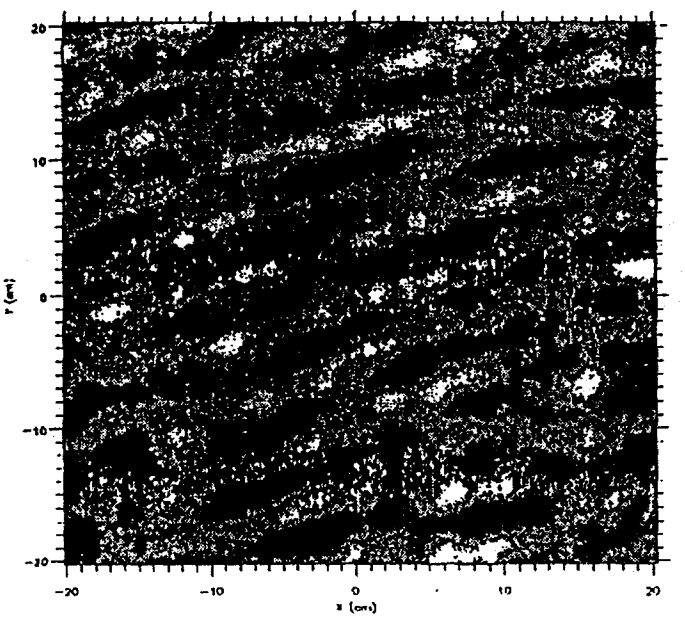

Figure 3. A gray-level plot of a synthesized phase map for an amplifier slab. This map was created from data sets of two sub-apertures.

3. SIMULATIONS OF BEAMLET 12 kJ/3 ns OPERATION AND COMPARISON WITH EXPERIMENT

Simulations have been made of Beamlet operating at an output energy of approximately 12 kJ (at 1.053 microns) in a temporally flat pulse of 3 ns duration. The modeling starts at the front end serrated aperture (Figure 2). The serrated aperture along with the subsequent spatial filter provides the initial beam apodization. Also in the front end is the gain compensator mask. This is a transmission mask with a parabolic shape. The ratio of maximum to minimum transmission is 3:1. The transmission varies only in the horizontal direction.

Figure 4 shows a calculated beam profile after the 5X spatial filter in the front end. The beam continues to have this "concave upwards" shape to a lesser and lesser degree until after the booster section at which point the beam central section is flat.

No aberrations were assigned to optical components in the front end section. In the main cavity and booster sections, each amplifier slab is assigned a pump-induced aberration and a static small-scale aberration phase map as is illustrated in Figure 3. The pump-induced aberrations used in the simulations vary in only 1 transverse dimension, that corresponding to the long dimension of the slab. Pump-induced aberrations are of large scale lengths (>2 cm). In addition, small scale phase maps are assigned to the cavity optical switch[5] and spatial filter

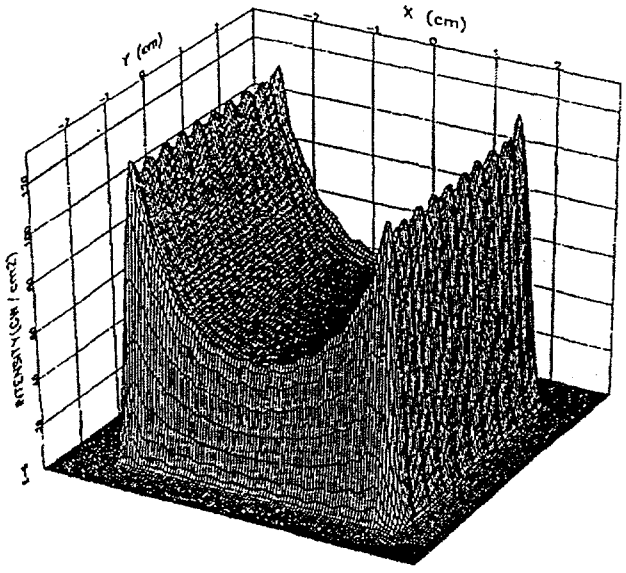

Figure 4. A 3D surface plot of the beam intensity after the gain compensator mask. The beam does not become flat in the central region until after the booster amplifier.

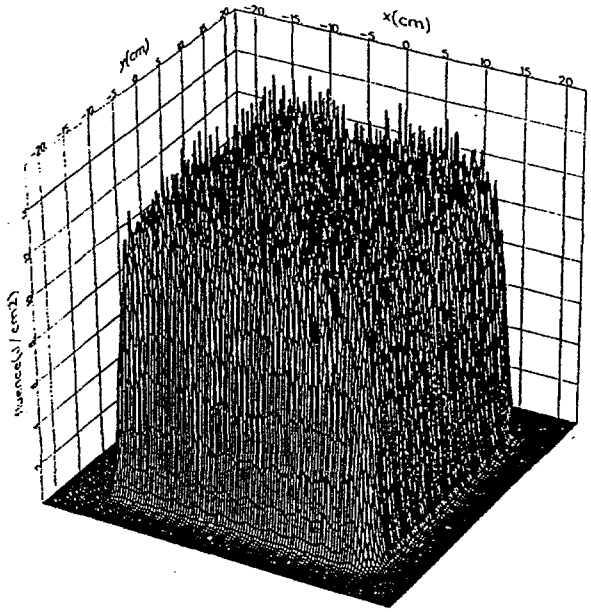

Figure 5. A 3D surface plot of the calculated 1ω fluence distribution of the beam at the frequency converter input. The flat central section of the distribution indicates the correct operation of the gain compensator mask.

lenses. The optical switch KDP crystal phase map contains regular structure due to the grooves made by the diamond turning machine.

Spatial filters in the modeling use the actual Beamlet cut-off angle of 200 μrad. These filters thus remove beam intensity and phase ripples with a scale length of less than 0.5 cm. At these cutoff angles, the modeling shows no noticeable clipping of energy by the pinholes.

Figure 5 shows a 3D surface plot of the fluence at the output of the 1ω section of Beamlet. Note the flat central section of the beam; this indicates that the gain compensator has operated as designed. The small scale modulation on the top section of the beam is due to the phase aberrations on the amplifier slabs. Diffraction and nonlinear index processes converted the phase ripples into amplitude ripples.

Since the Beamlet modeling does not utilize the exact set of optical component phase maps corresponding to an actual laser configuration, one cannot expect point by point agreement between calculated and measured beam distributions. In this situation, a statistical comparison needs to be made. Figure 6 shows a comparison between histograms for calculated and measured fluence distributions. The histogram for the calculated distribution shows a few points with a normalized fluence higher than the measured distribution histogram; otherwise the histograms are essentially identical.

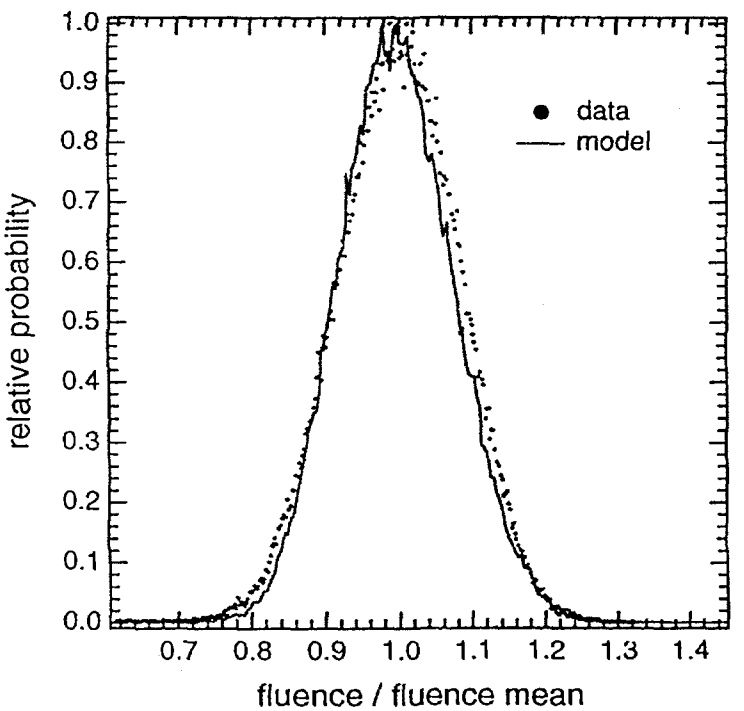

Figure 6. Plots of histograms for a calculated and measured near-field fluence distribution at the laser output for a 12 kJ/3 ns Beamlet shot.

Good statistical agreement also exists between measured and calculated 1ω far-field distributions. Figure 7 shows a comparison between the radial integrals of a calculated and measured 1ω far-field distribution. As can be seen from the figure, agreement is excellent. Another important to note is that there is a significant amount of far-field energy above 20 μrad. This contribution comes from the small-scale phase aberrations assigned to the amplifier slab and optical switch.

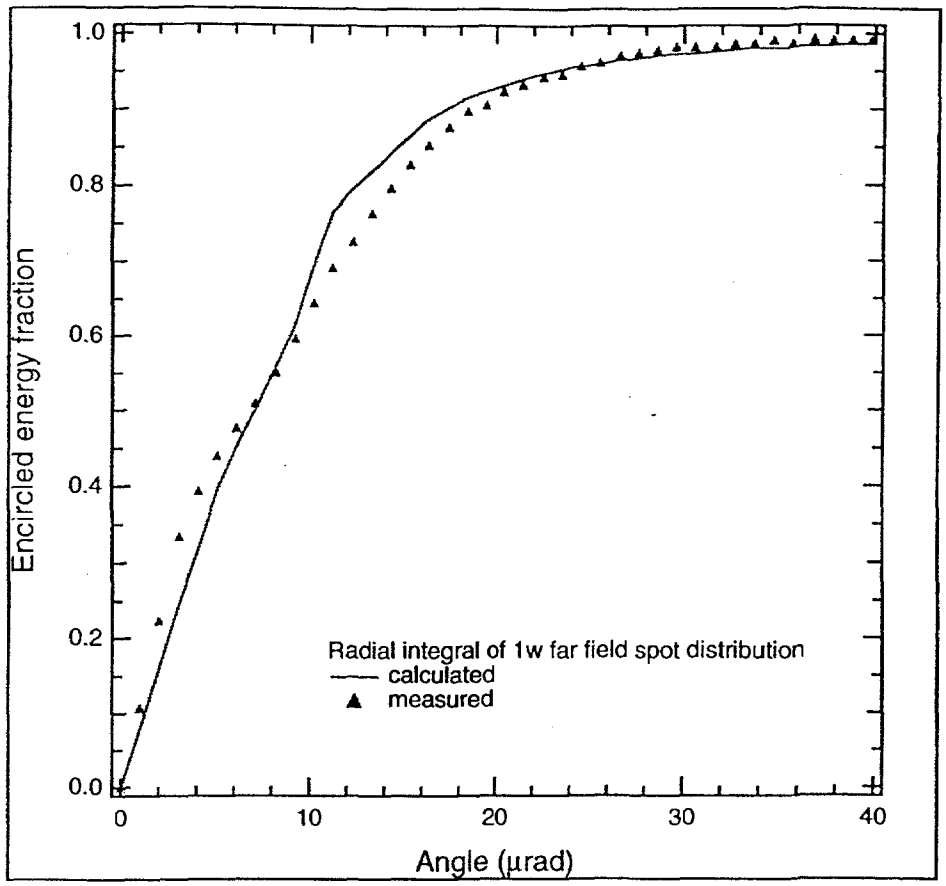

Figure 7. Plot of the radial integral of a calculated 1ω far-field distribution and several points from the radial integral of a measured 1ω far-field distribution.

The excellent agreement for both near-field and far-field statistics can be attributed to the use of measured phase aberration data for the optical components. In other words, the quality of the modeling output is as good as the quality of the modeling input.

4. ACKNOWLEDGMENTS

We acknowledge the efforts of Dr. D.R. Speck, Derek Decker and the Beamlet Diagnostics team in providing the data for comparison with our calculations. We also acknowledge the efforts of C.R. Wolfe and M. Kellan who made the many interferometric measurements of the optical components and then processed that data to obtain phase maps. We appreciate the many discussions with Dr. J.B. Trenholme and Dr. J.T. Hunt.

This work was performed under the auspices of the US Department of Energy by the Lawrence Livermore National Laboratory under Contract No. W-7405-ENG-48.

5. REFERENCES

1. J.F. Holzrichter, D. Eimerl, E.V. George, J.B. Trenholme, W.W. Simmons, and J.T. Hunt, "Physics of Laser Fusion, Volume III, High-Powered Pulse Lasers," 22-36, Lawrence Livermore National Laboratory UCRL-52868 Rev. 1 (1982).

2. L.M. Frantz, J.S. Nodvik, "Theory of pulse propagation in a laser amplifier," *J. Appl. Phys.* 14, 2346 (1963)

3. A.C. Erlandson, K.S. Jancaitis, R.W. Mc Cracken, M.D. Rotter, "ICF Quarterly Report," 2(3), 105-114, Lawrence Livermore National Laboratory, Livermore, CA, UCRL-LR-105821-92-1 (1992)

4. Jerome M. Auerbach, Victor P. Karpenko, "Serrated-aperture apodizers for high-energy laser systems," *Appl. Optics*, 33(15), 3179-3183, (1994)

5. M.A. Rhodes, J.J. De Yoreo, B.W. Woods, and L.J. Atherton, "ICF Quarterly Report," 2(1), 23-36, Lawrence Livermore National Laboratory, Livermore, CA UCRL-LR-105821-92-1